Adsorbate Interactions of Paramagnetic Palladium(I) Species in Pd(II)-Exchanged Na−MCM-22 Zeolite

A. M. Prakash, Tomasz Wasowicz,† and Larry Kevan*

Department of Chemistry, University of Houston, Houston, Texas 77204-5641

Received: November 5, 1996; In Final Form: January 20, 1997[⊗]

Adsorbate interactions of paramagnetic palladium(I) species in Pd(II)-exchanged Na−MCM-22 zeolite are studied by electron spin resonance (ESR) and electron spin-echo modulation (ESEM) spectroscopies. Oxidation and subsequent evacuation at 825 K of Na−MCM-22 zeolite exchanged with $Pd(NH_3)_4Cl_2$ results in the formation of a Pd(I) species. Monovalent palladium can be produced in PdNa−MCM-22 material by room temperature hydrogen reduction after dehydration and O_2 treatment at high temperature. Addition of hydrogen to PdNa−MCM-22 after dehydration, O_2 treatment, and evacuation (activation) is found to increase the concentration of Pd(I) at room temperature and at higher temperature is found to reduce Pd(I) to $Pd(0)_n$ (palladium clusters). Adsorption of O_2 and H_2O to an activated sample containing Pd(I) generates a Pd(II)−O_2^- species with $g_\perp > g_\parallel$. Adsorption of CO on an activated sample results in a Pd(I)−$(CO)_2$ complex which partially transforms to Pd(I)−CO on evacuation. Adsorption of ethylene on an activated sample produces Pd(I)−C_2H_4 and Pd(I)−C_4H_8 complexes, suggesting that Pd(I) catalyzes dimerization of ethylene. Methanol and ethanol behave differently when adsorbed on an activated sample. While methanol reduces Pd(I) to $Pd(0)_n$ at room temperature, ethanol forms a palladium complex suggested to be Pd(I)−CH_3CH_2OD. Adsorption of ammonia on activated PdNa−MCM-22 leads to two Pd(I)−$(ND_3)_1$ complexes, probably in different environments. On the other hand, adsorption of pyridine results only in a single species, perhaps due to steric effects. The kinetic size of the adsorbates plays a major role in forming complexes with Pd(I) in MCM-22 zeolite. A significant amount of Pd(I) formed during activation is located in sites inaccessible to relatively large molecules while it reacts immediately with smaller adsorbates.

Introduction

Zeolite MCM-22 is a novel molecular sieve discovered recently by scientists at Mobil.[1−3] High thermal stability, large sorption capacity, and high surface area render this material very interesting for catalysis. MCM-22 in its acidic form has been claimed to be a useful catalyst for isoalkane/olefin alkylation, skeletal and double bond isomerization in olefins, and the conversion of methanol or olefins to higher hydrocarbons.[4] The modification of this material by incorporation of transition metal ions in either framework or extraframework positions is of potential significance for specific catalytic reactions. Pt- or Pd-modified MCM-22 is a useful catalyst for the conversion of parafins to olefins and/or aromatics.[5] In particular, Pt/MCM-22 is reported to be very efficient for the production of high density, cycloparafin-rich jet fuel.[6] Copper or rare earth modified MCM-22 materials are found to reduce CO and NO/NO_2 emissions from refineries when it is added to a USY catalyst.[7] However, no systematic study of transition metal ion incorporation in MCM-22 zeolite has been reported. Recently, we studied the formation and adsorbate interactions of paramagnetic nickel (I) in Ni(II)-exchanged Na−MCM-22 zeolite.[8]

Pd(II) ions have been incorporated into extraframework sites in zeolites and other molecular sieves by liquid phase and solid state ion exchange.[9,10] Substitution of Pd(II) into framework sites of zeolites has not been reported so far. Several characterization techniques such as electron spin resonance (ESR), X-ray diffraction (XRD), infrared spectroscopy, and X-ray photoelectron spectroscopy have been employed to identify the location and the specific oxidation state of palladium in zeolites.[9−14] ESR is found to be useful in identifying paramagnetic Pd ions such as Pd(I) and Pd(III). Electron spin-echo modulation (ESEM) spectroscopy, when combined with ESR, is found to be very effective in providing additional quantitative information concerning adsorbate geometry in terms of the number of surrounding adsorbate nuclei (N) and their interaction distance (R).[15] Depending on the sample pretreatment, both Pd(I) and Pd(III) can be stabilized in zeolite with a relatively high negative framework charge such as in X and Y zeolites.[9,12] However, in high silica zeolites and silicoaluminophosphate (SAPO) molecular sieves Pd(I) seems to be the only paramagnetic oxidation state stabilized which is likely associated with the relatively low negative framework charge.[10,16,17] Zeolite-supported Pd(I) catalysts are active for hydrocracking,[18] hydrogenation,[19] and dimerization of small olefins.[20,21] The activity of the catalyst depends on several factors such as the structure type, the environment, the location, and the ion concentration. The structural features of the host zeolite matrix have direct influence on the site location of the paramagnetic species and their coordination geometries with adsorbates. Due to the unusual structural aspects of MCM-22 zeolite, transition metal ion-modified MCM-22 catalysts are expected to have specific activity and selectivity behavior in various reactions. Therefore, we initiated a systematic study of palladium incorporation into Na−MCM-22 zeolite. Monovalent palladium has been stabilized in Na−MCM-22 zeolite. Pd(I) complexes with various molecules have been studied in order to provide a better understanding of Pd(I) interactions with various adsorbates of catalytic interest. ESR and ESEM spectroscopies are used to monitor the formation of Pd(I) and its interaction with various adsorbates in PdNa−MCM-22.

† On leave from the Institute of Nuclear Chemistry and Technology, ul. Dorodna 16, 03-195 Warsaw, Poland.

⊗ Abstract published in *Advance ACS Abstracts,* February 15, 1997.

S1089-5647(96)03455-4 CCC: $14.00

Experimental Section

Sample Preparation. MCM-22 zeolite was prepared according to a modified procedure developed in our laboratory. The procedure for the synthesis of MCM-22 has been reported elsewhere.[8] The as-synthesized sample was calcined by slowly raising the temperature to 823 K in nitrogen and then holding at this temperature for 16 h in oxygen for removal of the organic template. Palladium was introduced into the zeolite as $Pd(NH_3)_4^{2+}$ cation by exchange with palladium tetramine chloride (Alpha). About 250 mg of calcined Na−MCM-22 zeolite was ion-exchanged with 50 mL of 0.01 M $Pd(NH_3)_4Cl_2 \cdot H_2O$ at 295 K for 24 h. The filtered and washed material was dried in air at room temperature. Before and after ion exchange, the color of the sample remained white.

Sample Treatment and Measurements. X-ray powder diffraction patterns were recorded on a Siemens D5000 X-ray diffractometer using Cu Kα radiation. Thermogravimetric (TG) analysis were carried out in O_2 on a Dupont 957 thermal analyzer at a heating rate of 10 K/min. Morphology and particle size of MCM-22 samples were studied by scanning electron microscopy. Chemical analysis of the samples was carried out by electron microprobe analysis on a Jeol JXA-8600 spectrometer. For ESR and ESEM studies, PdNa−MCM-22 samples were loaded into 3 mm o.d. by 2 mm i.d. Suprasil quartz tubes and evacuated at room temperature for about 16 h. To study the behavior of the palladium as a function of hydration, a sample was slowly heated from room temperature to 373, 473, 573, 673, and 773 K in vacuum. For each interval, the temperature was raised slowly and held at this temperature for 16 h. ESR spectra were then measured at 77 K to detect any paramagnetic Pd species produced by this thermal treatment. In another treatment the samples were evacuated at room temperature for 16 h. While in vacuum, the temperature was slowly raised to 823 K over a time of 6 h and then held at this temperature for 16 h before cooling to room temperature. This gives a type A sample. Type A samples were then heated in 300 Torr of dry oxygen at 823 K for 5 h to give a type B sample. Type B samples were evacuated at 823 K for 16 h to give activated samples termed type C. Both type A and type B samples show no ESR signal, while type C samples show a strong ESR signal identified as Pd(I). In order to prepare Pd(I) complexes with various adsorbates, type C "activated" samples were exposed to H_2, O_2, CO (MSD Isotopes), C_2D_4 (Union Carbide), and ND_3 (Stohler Isotope Chemicals) at about 300 Torr and to the room temperature vapor pressure of D_2O (Aldrich), CH_3OD (Stohler Isotope Chemicals), CH_3CH_2OD (Aldrich), and C_2D_5N (pyridine) (Aldrich). These samples with adsorbates were frozen in liquid nitrogen and sealed before ESR and ESEM measurements.

ESR spectra were recorded with a Bruker ESP 300 X-band spectrometer at 77 K. The magnetic field was calibrated with a Varian E-500 gaussmeter. The microwave frequency was measured by a Hewlett-Packard HP 5342A frequency counter. ESEM spectra were measured at 4.5 K with a Bruker ESP 380 pulsed ESR spectrometer. Three pulse echoes were measured by using a $\pi/2-\tau-\pi/2-T-\pi/2$ pulse sequence as a function of time T to obtain the time domain spectrum. Both the theory and methods used for ESEM measurements and simulation of the data are described in detail elsewhere.[15] To minimize ^{27}Al and ^{29}Si modulation from framework aluminum and silicon in measurements of deuterium modulation, the τ value was fixed accordingly depending on the magnetic field position. The deuterium modulations were analyzed by a spherical approximation for powder samples in terms of N nuclei at distance R with an isotopic hyperfine coupling A_{iso}.[15] The best fit simulation of an ESEM signal is found by varying the parameters until the sum of the squared residuals is minimized.

Results

Zeolite MCM-22 was prepared under hydrothermal conditions using hexamethyleneimine as the structure directing agent. Samples were prepared by both agitated and nonagitated batch synthesis. The as-synthesized product (MCM-22 precursor) is of unknown structure and undergoes a change in structure upon calcination at about 810 K to yield MCM-22 zeolite.[2] X-ray powder diffraction patterns recorded on as-synthesized and calcined forms match well with the corresponding patterns reported in the literature for this material.[8] Highly crystalline samples were obtained as revealed by XRD. The crystal morphology of MCM-22 is essentially the same as that reported, but the crystallite size is considerably larger. When synthesis is carried out with agitation, MCM-22 zeolite crystallizes in small discs or platelets with a diameter below 1 μm and a thickness about 0.1 μm, occasionally forming spherical aggregates of 6−8 μm. For synthesis with nonagitation, the product crystallites typically are small platelets about 4−6 μm across. Occasionally, several such platelets are bunched together to form clusters of larger size. The platelets are almost always intergrown. The chemical composition of MCM-22 was determined by electron microprobe analysis. Samples prepared with nonagitation are used for the present investigation and have a SiO_2/Al_2O_3 ratio equal 22.4 for as-synthesized samples. The molar chemical composition of a palladium-exchanged sample is 1.00 Al_2O_3:23.42 SiO_2:0.83 PdO:0.01 Na_2O based on electron microprobe microanalysis. Note that the SiO_2/Al_2O_3 ratio of this material is higher than that of the original MCM-22 sample used for calcination and subsequent ion exchange. Dealumination due to calcination has been already reported in MCM-22 zeolite.[22]

ESR Measurements. The dehydration behavior under vacuum of PdNa−MCM-22 zeolite was studied versus temperature. Dehydration of PdNa−MCM-22 at 295 K for 16 h does not show any ESR signal at 77 K. Thus, the Pd species exist in the form of Pd(II). Dehydration at 373 K for 16 h, however, produces a weak species A with $g_\perp = 2.130$. A second species with $g = 2.042$ is also observed at this temperature. Species A is probably due to Pd(I) formed by thermal decomposition of $[Pd(NH_3)_4]^{2+}$ and reduction of Pd(II) by ammonia or desorbing water. Both species disappear almost completely on dehydration at 473 K for 16 h. The second species with $g = 2.042$ may possibly be due to crystal defects.[23] Dehydration at higher temperatures does not show any ESR signals indicating that any Pd(I) formed is further oxidized to Pd(II) at higher temperature. It has been reported that thermal decomposition of $[Pd(NH_3)_4]^{2+}$ begins under vacuum at 373 K.[13] Raising the treatment temperature to 523 K causes further decomposition of the cation complex.

Evacuation with slowly increasing temperature to 823 K (type A sample), oxidation with static oxygen at the same temperature (type B sample), and evacuation again at 823 K (type C sample) produce dark brown, chocolate brown, and ash gray samples successively. While type A and B samples show no ESR signal, type C samples produce an axially symmetric ESR signal (Figure 1a). Degassing of type B samples at room temperature does not produce paramagnetic palladium species detectable by ESR. Species B observed after activation (type C sample) has been assigned to Pd(I) formed by thermal reduction in several palladium-modified zeolites and other molecular sieves including zeolite X,[9] Y,[12] mordenite,[13] SAPO-5,[16] SAPO-11,[10] and SAPO-34.[17]

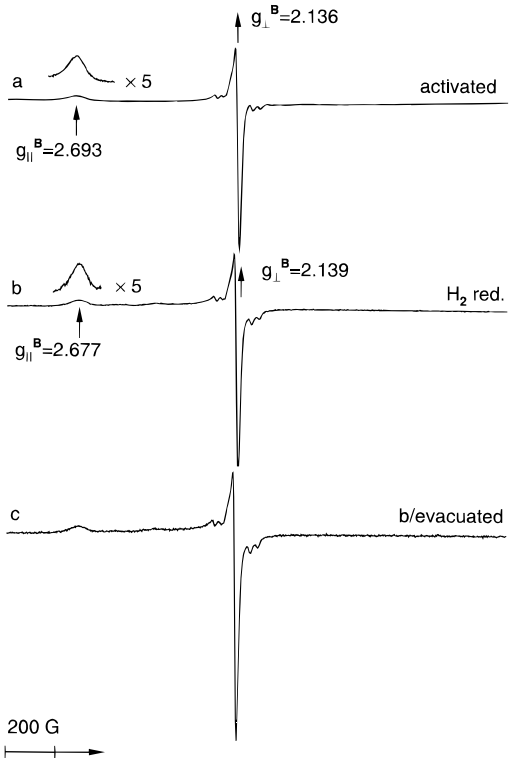

Figure 1. ESR spectra at 77 K of PdNa−MCM-22 zeolite (a) after dehydration, oxidation, and subsequent evacuation at 823 K (sample type C); (b) after dehydration, oxidation, and subsequent reduction in H_2 (70 Torr) at 295 K; (c) after evacuation of an H_2 reduced sample at 295 K for 30 min.

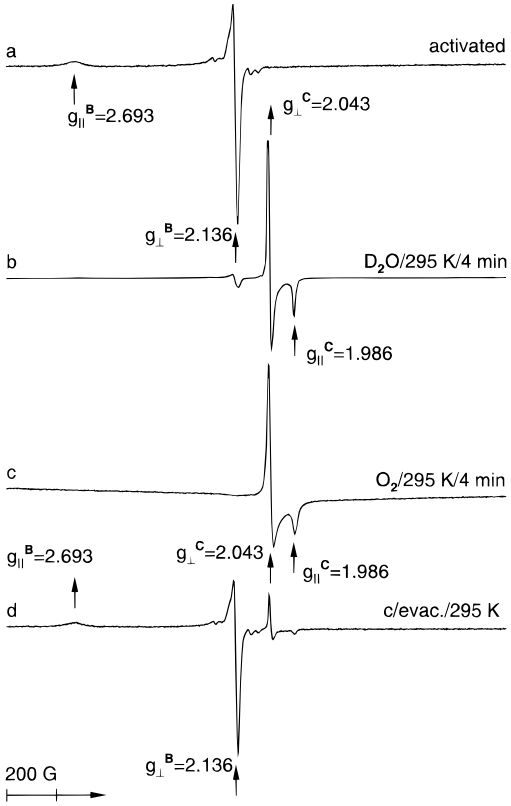

Figure 2. ESR spectra at 77 K of PdNa−MCM-22 zeolite (a) after activation, (b) after D_2O adsorption on an activated sample at 295 K for 4 min, (c) after 100 Torr of O_2 adsorption on an activated sample, and (d) after evacuation of an O_2-treated sample at 295 K for 20 min.

The reduction behavior of PdNa−MCM-22 zeolite in the presence of H_2 was also studied. An ESR spectrum similar to that observed for a type C sample is observed when a type B sample is evacuated and treated with dry hydrogen (70 Torr) at room temperature (Figure 1b). The color of the sample is also changed from chocolate brown to ash gray during this process. We assign this species to Pd(I) formed by hydrogen reduction. Hydrogen treatment at room temperature for a very short duration (about 2 min) is sufficient for producing Pd(I).

The effect of added oxygen and water to activated samples showing Pd(I) signals was studied in Figure 2. Adsorption of both dry oxygen (100 Torr) and D_2O on activated samples for 4 min gives a new axially symmetric ESR signal, denoted as C, with reversed **g** tensors ($g_\perp = 2.043$ and $g_\parallel = 1.986$). Whereas species B disappears completely after 4 min of oxygen adsorption at room temperature, a small fraction of species B is still visible in a sample with adsorbed D_2O. The behavior of these samples on further evacuation at room temperature is, however, different. In a sample with adsorbed oxygen, about 20 min of evacuation at room temperature is sufficient to regenerate species B (Figure 2d). However, in a sample with adsorbed D_2O, 20 min of evacuation at room temperature does not change the ESR spectrum. This difference in behavior of the two samples suggests that although species C has the same ESR characteristics in both cases, the mode of formation of species C is different in these two samples.

The effect of hydrogen treatment on an activated sample containing Pd(I) was investigated in Figure 3. When 80 Torr of dry hydrogen is exposed to activated PdNa−MCM-22, an ESR spectrum similar to that observed on an activated sample is observed. However, the intensity of species B is increased by a factor of 10 by the hydrogen treatment based on double integration. Upon heating the hydrogen treated sample at 573 K for 30 min, the intensity of species B reduces considerably

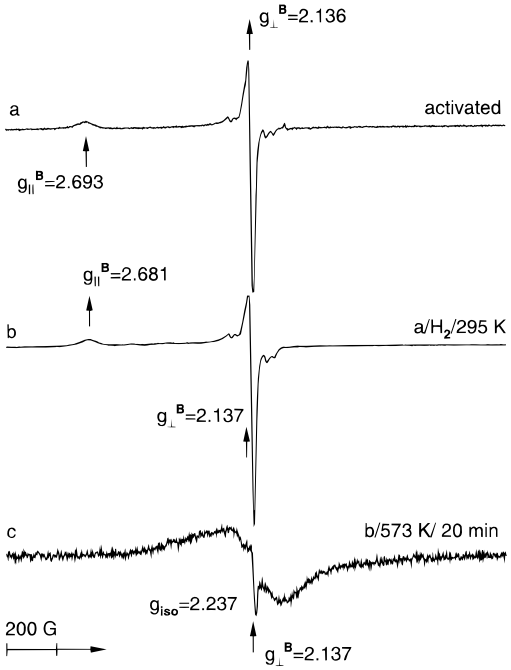

Figure 3. ESR spectra at 77 K of PdNa−MCM-22 zeolite (a) after activation, (b) after 80 Torr of H_2 adsorption on an activated sample at 295 K for 4 min, and (c) after heating an H_2 adsorbed sample at 573 K for 20 min.

with concomitant formation of a broad isotropic ESR signal at $g = 2.237$ assigned to palladium clusters. Thus, at high temperature hydrogen reduces Pd(I) to $Pd(0)_n$.

The interaction of CO and Pd(I) in PdNa−MCM-22 was studied in Figure 4. When 70 Torr of ^{12}CO (^{12}C has zero nuclear spin) is adsorbed on an activated sample at room

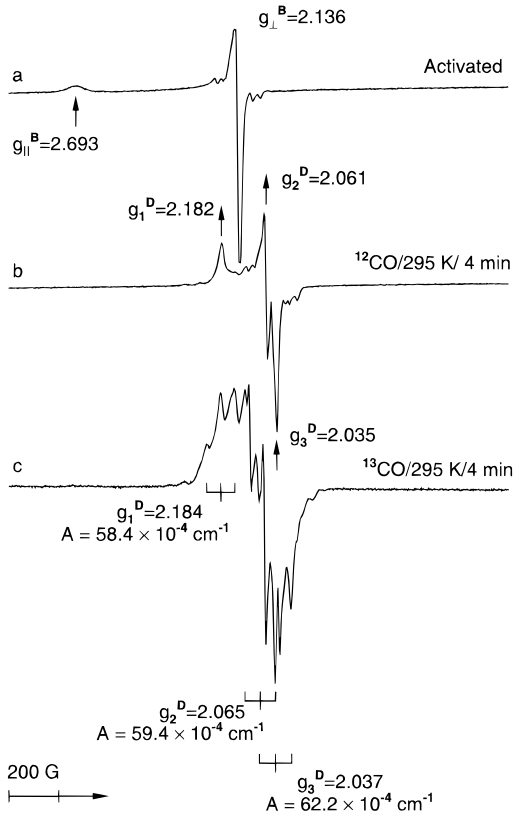

Figure 4. ESR spectra at 77 K of PdNa−MCM-22 zeolite (a) after activation, (b) after 70 Torr of ^{12}CO adsorption on an activated sample at 295 K for 4 min, and (c) after 70 Torr of ^{13}CO adsorption on an activated sample at 295 K for 4 min.

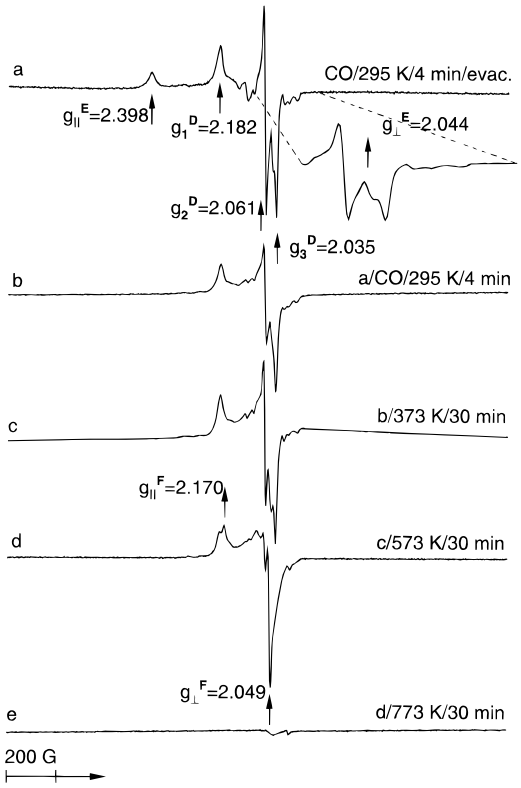

Figure 5. ESR spectra at 77 K of PdNa−MCM-22 zeolite after adsorption of ^{12}CO (70 Torr) on an activated sample (a) after evacuation at 295 K for 20 min, (b) after readsorption of 70 Torr of ^{12}CO on the evacuated sample at 295 K for 4 min, and after heating the CO adsorbed sample at (c) 373 K for 30 min, (d) 573 K for 30 min, and (e) 773 K for 30 min.

temperature, signal B disappears, and a new species, denoted as D, is immediately observed, apparently due to the coordination of ^{12}CO to Pd(I). The g values of species D are $g_1 = 2.182$, $g_2 = 2.061$, and $g_3 = 2.035$ as shown in Figure 4b. When 70 Torr of ^{13}CO (^{13}C has a nuclear spin of $^1/_2$) is added to an activated sample at room temperature, a more complex ESR pattern is observed with three sets of resolved triplets (Figure 4c). Each triplet is centered around g_1, g_2, g_3 with relative intensities of 1:2:1. Hyperfine splittings for g_1, g_2, and g_3 are $(60 \pm 2) \times 10^{-4}$ cm^{-1}.

Species D is quite stable at room temperature. The intensity of this signal remains unchanged after keeping the sample at room temperature for 24 h. However, upon evacuating the sample for 20 min the intensity of this species decreases and a second species E appears in the ESR spectrum (Figure 5a). This second species E has an axial **g** tensor with $g_{||} = 2.398$ and $g_\perp = 2.044$. Species E disappears on CO adsorption with a concomitant increase in the intensity of species D (Figure 5b). On annealing the sample at higher temperatures, species D gradually transforms to species F (Figure 5d) at 573 K. Species F has axial g values with $g_{||} = 2.170$ and $g_\perp = 2.049$.

When ethylene (100 Torr) is adsorbed on an activated sample at room temperature, several new signals are observed as shown in Figure 6. Three signals, designated as species G_1, G_2, and G_3 with separate $g_{||}$ values (2.397, 2.312, and 2.229) and similar $g_\perp$ values (2.011, 1.994, and 1.989), are the main features of the spectrum. Another species H with $g_\perp = 2.044$ is also observed after ethylene adsorption. Annealing the sample at room temperature increases the intensity of species H; otherwise, the spectrum remains the same. However, on heating the sample at 353 K the spectrum changes considerably. Species G changes to a rhombic signal with $g_1 = 2.009$, $g_2 = 2.003$, and $g_3 = 1.994$. Also, a new species I appears with $g_\perp = 2.086$ and with a concomitant decrease in the intensity of species H. On further heating to 423 K, species I decreases its intensity and disappears almost completely for longer heating at this temperature (Figure 6d). At the same time species G completely decays, and an isotropic signal with $g = 2.003$ appears in the spectrum.

Room temperature adsorption of methanol and ethanol on PdNa−MCM-22 result in entirely different ESR spectra shown in Figure 7. Adsorption of CH_3CH_2OD for 4 min on an activated sample generates a new species J characterized by $g_{||} = 2.606$ and $g_\perp = 2.108$ as shown in Figure 7b. At the same time the intensity of species B reduces to about 40% of its original intensity. Species C observed after ethanol adsorption is due to some water impurity present. When CH_3OD is added to an activated sample, a broad, isotropic species K with $\Delta H_{pp} \sim 155$ G at $g = 2.142$ is observed with a concomitant reduction in the intensity of species B (Figure 7c). The essential features of the spectrum remain unchanged, although a slight reduction in the intensity of B is observed upon annealing the sample at room temperature for 24 h (Figure 7d). In previous work,[24] such a broad isotropic ESR signal was attributed to the formation of small palladium clusters $Pd(0)_n$ formed by the reduction of Pd(I) by methanol. Note that a species similar to K is observed when PdNa−MCM-22 is treated with hydrogen at 573 K. The fact that species K is absent when ethanol is adsorbed on a similar sample indicates a lower reduction capability for ethanol.

ESR spectra of activated PdNa−MCM-22 after adsorption of ammonia and pyridine are shown in Figure 8. Upon adsorption of ammonia two species L and M appear as shown in Figure 8b. Both species L and M have axially symmetric **g** tensors with values $g_{||} = 2.358$, $g_\perp = 2.076$ and $g_{||} = 2.405$, $g_\perp = 2.007$, respectively. Species L also shows anisotropic nitrogen hyperfine splitting values of $A_{||} = 0.003\,52$ cm^{-1} and

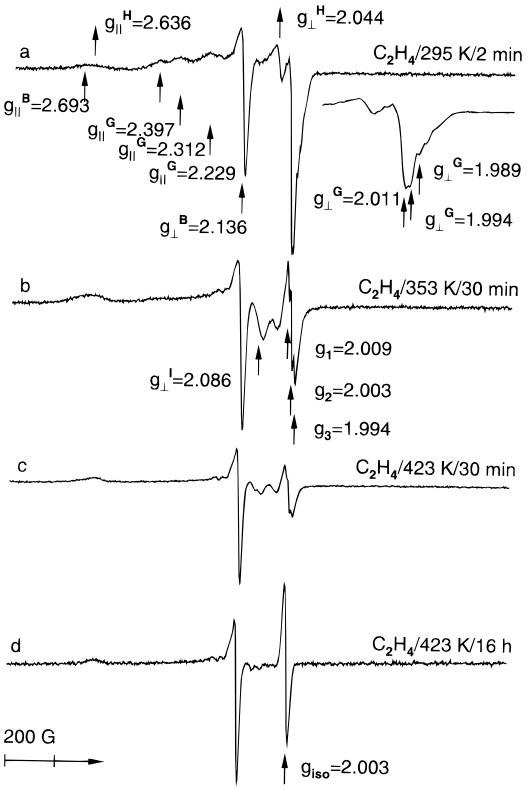

Figure 6. ESR spectra at 77 K of PdNa−MCM-22 zeolite after adsorption of ethylene (100 Torr) on an activated sample (a) after 2 min of ethylene adsorption at 295 K, (b) after heating the ethylene adsorbed sample at 353 K for 30 min, (c) after subsequently heating the ethylene adsorbed sample at 423 K for 30 min, and (d) after heating the ethylene adsorbed sample at 423 K for 16 h.

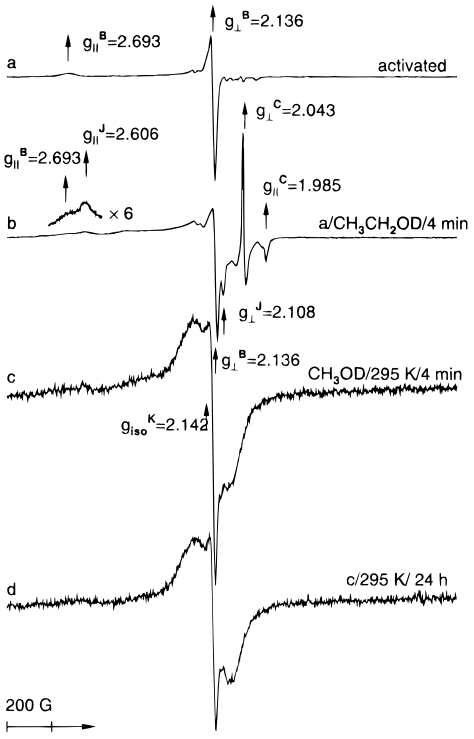

Figure 7. ESR spectra at 77 K of PdNa−MCM-22 zeolite (a) after activation,(b) after CH_3CH_2OD adsorption on an activated sample at 295 K for 4 min, (c) after CH_3OD adsorption on an activated sample at 295 K for 4 min, and (d) after annealing a methanol adsorbed sample at 295 K for 24 h.

$A_{\perp} = 0.001\ 48\ cm^{-1}$. When pyridine is adsorbed, a new species N together with species C is observed. Species N has $g_{\parallel} =$

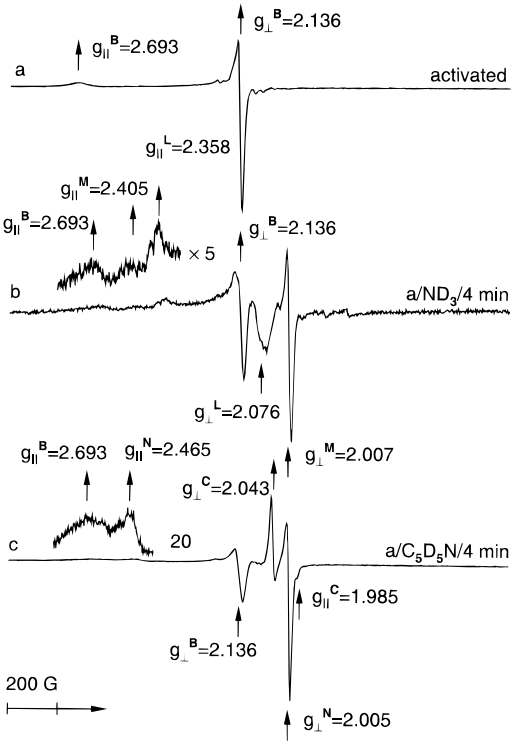

Figure 8. ESR spectra at 77 K of PdNa−MCM-22 zeolite (a) after activation, (b) after ND_3 adsorption on an activated sample at 295 K for 4 min, and (c) after C_5D_5N adsorption on an activated sample at 295 K for 4 min.

2.465 and $g_{\perp} = 2.005$. Both species M and N have similar ESR characteristics, although their g values differ slightly. These species do not show any nitrogen hyperfine splitting.

Table 1 summarizes the ESR parameters and suggested assignments of the various Pd species observed on PdNa−MCM-22 with various adsorbates.

ESEM Measurements. Electron spin echo modulation measurements are useful in identifying the adsorbate geometry of paramagnetic metal ion complexes with various molecules. Three-pulse ESEM measurements of deuterium modulation of Pd(I) were performed on activated PdNa−MCM-22 after adsorbing various deuterated inorganic and organic molecules at 295 K. Measurements were done at 4.5 K. Figure 9 shows the experimental and simulated spectra obtained for Pd(I) in a type C activated sample of PdNa−MCM-22 with adsorbed D_2O. The magnetic field was set at the $g_{\perp}$ of species B and C (Figure 2b). The time between the first two pulses was set to 280 ns to optimize deuterium modulation. Simulation of the spectrum at $g_{\perp}$ for species B indicates two deuterium nuclei at a distance of 0.42 nm. Similarly, simulation of the spectrum at $g_{\perp}$ for species C indicates two deuterium nuclei at a distance of 0.44 nm. Both values indicate a weak interaction of one water molecule with both species B and C, since the observed distance is much larger than for water directly coordinated to Pd(I). The ESEM parameters are summarized in Table 2.

The three-pulse ESEM spectra for an activated sample with adsorbed C_2D_4 are not shown, but the parameters are in Table 2. The ESR spectrum after adsorption of C_2D_4 is the same as the ESR spectrum after adsorption of C_2H_4 (Figure 6b). The magnetic field was set at $g_{\perp}$ of species G and species B. The spectrum observed for species G could be best simulated with four deuterium nuclei at a distance of 0.37 nm. This value is consistent with a π-bonding interaction of Pd(I) with one ethylene molecule. The spectrum observed for species B shows four deuterium nuclei at 0.50 nm in a first shell and another

TABLE 1: ESR *g* Values of Paramagnetic Pd Species in PdNa−MCM-22 Formed during Various Reduction Treatments and after Adsorbing Various Inorganic and Organic Molecules

treatment	adsorbate	species	assignment	g_{iso} or $g_{\|}$ or g_1[a]	$g_\perp$ or g_2[a]	g_3[a]
dehydrated		A	Pd(I)	2.130		
activated		B	Pd(I)	2.693	2.136	
H_2 reduced		B	Pd(I)	2.677	2.139	
activated	H_2 (295 K)	B	Pd(I)	2.681	2.137	
	H_2 (573 K)	K	$Pd(0)_n$	2.237		
activated	O_2	C	$Pd(II)-O_2^-$	1.985	2.043	
activated	D_2O	C	$Pd(II)-O_2^-$	1.986	2.043	
activated	CO	D[b]	$Pd(I)-(CO)_2$	2.182	2.061	2.035
		E	$Pd(I)-(CO)_1$	2.398	2.044	
activated	C_2H_4	G_1	$Pd(I)-(C_2H_4)_1$	2.397	1.934	
		G_2	$Pd(I)-(C_2H_4)_1$	2.312	1.929	
		G_3	$Pd(I)-(C_2H_4)_1$	2.230	1.921	
		H	$Pd(I)-(C_4H_8)_1$	2.636	2.047	
activated	CH_3OD	K	$Pd(0)_n$	2.142		
activated	C_2H_5OD	J	$Pd(I)-(C_2H_5OD)_1$	2.606	2.108	
activated	ND_3	L[c]	$Pd(I)-(ND_3)_1$	2.358	2.076	
		M	$Pd(I)-(ND_3)_1$	2.405	2.007	
activated	C_5D_5N	N	$Pd(I)-(C_5D_5N)_1$	2.465	2.005	

[a] Estimated uncertainty is ±0.008. [b] Species D observed after ^{13}CO adsorption shows ^{13}C hyperfine splitting with $A_{iso} = 60 \times 10^{-4}$ cm^{-1}. [c] Species L shows ^{14}N hyperfine splitting with $A_{\|} = 35 \times 10^{-4}$ cm^{-1} and $A_\perp = 15 \times 10^{-4}$ cm^{-1}.

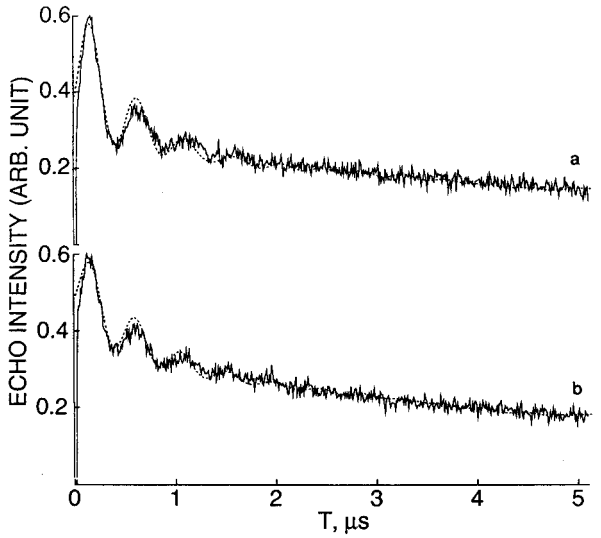

Figure 9. Experimental (—) and simulated (···) three-pulse ESEM spectra at 4.5 K on an activated PdNa−MCM-22 sample after adsorbing D_2O at 295 K for 4 min. Spectra were measured at the magnetic field corresponding to (a) $g_\perp$ of species C and (b) $g_\perp$ species B.

TABLE 2: Three-Pulse ESEM Parameters of Paramagnetic Pd Species in PdNa−MCM-22 Zeolite with Adsorbates

adsorbate	species	N[a]	R,[b] nm	A,[c] MHz
D_2O	C	2	0.45	0.05
	B	2	0.43	0.05
C_2D_4	G	4	0.45	0.05
	B	4	0.50	0.05
		4	0.65	0
CH_3CH_2OD	J	1	0.28	0.20
	B	1	0.45	0.05
ND_3	L	3	0.30	0.15
	M	3	0.40	0.07
	B	3	0.45	0.05
C_5D_5N	N	2	0.40	0.05
		2	0.60	0
	B	4	0.48	0.05

[a] Number of deuterium atoms. [b] Distance beteween Pd and deuterium, estimated uncertainity is ±0.02 nm. [c] Isotropic hyperfine coupling constant; estimated uncertainty is ±10%.

four deuterium nuclei at 0.68 nm in a second shell. These values are too large for direct coordination of ethylene with Pd(I).

The ESEM spectra for an activated sample after CH_3CH_2-OD adsorption were also studied and the parameters are in Table 2. The magnetic field was set at $g_\perp$ of species J and B (Figure 7b). Measurements on both species J and B involve some contributions from the other species as evident from the echo-detected ESR spectrum. Nevertheless, simulation of the spectrum for species J seems approximately valid for one deuterium at 0.3 nm which is indicative of one ethanol molecule coordinated to Pd(I). The deuterium modulation for species B is too weak to be analyzed. ESEM measurements were not attempted after adsorption of deuterated methanol because of greater superposition of species K and B (Figure 7c).

The three-pulse ESEM spectra for an activated sample after adsorption of ND_3 are fit by the parameters in Table 2. The magnetic field was set at the $g_\perp$ of species L, M, and B (Figure 8b). For species L, simulation of the spectrum gives three deuterium nuclei at 0.30 nm. This corresponds to an interaction of one ND_3 molecule with Pd(I) to form species L. Simulation of the spectrum for species M gives three deuterium nuclei at 0.40 nm. This also corresponds to the coordination of one ND_3 molecule with Pd(I).

Three-pulse ESEM spectra obtained after adsorption of C_5D_5N on an activated sample give the parameters shown in Table 2. The field was set on the $g_\perp$ of species N as well as on the $g_\perp$ of species B. For species N simulation gives two deuteriums at 0.4 nm in a first shell and two nuclei at 0.6 nm for the second shell. It should be noted that measurements of species N may include contributions from species C based on the echo-detected ESR. These parameters indicate that one pyridine molecule is coordinated to Pd(I) to form species M. The ESEM spectrum for species B also shows some weak deuterium interactions.

Discussion

Structure. MCM-22 is a high silica zeolite which can be prepared over a range of Si/Al ratios. The structure of MCM-22 proposed recently by Leonowicz et al.[3] contains interesting features. The structure is composed of interconnected $\{4^3 5^6 6^3$-$[4^3]\}$ building units forming two independent pore systems, both of which are accessed through rings composed of 10 tetrahedral (T) atoms. One of these pore systems is defined by two-dimensional sinusoidal channels. The other consists of large super cages defined by 12 T atoms with an inner free diameter of 7.1 Å and inner height of 18.2 Å.

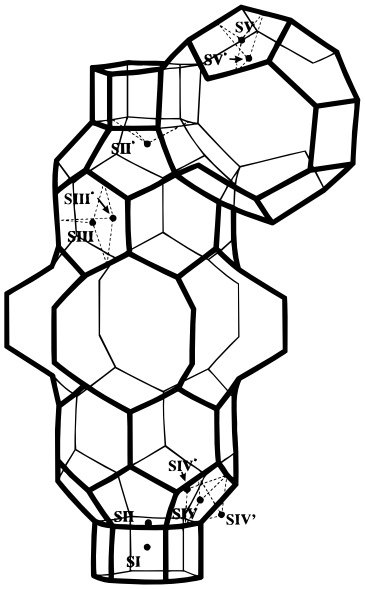

Figure 10. Possible cation sites and their designation in MCM-22 zeolite (see text for description).

In MCM-22 several potential cation sites have been suggested.[3] On the basis of the proposed structural model of MCM-22 and by analogy with the cation sites in X and Y zeolites,[25] probable cation sites in MCM-22 are shown in Figure 10. Sites SI through SIV are associated with the supercage, and site SV is associated with the interlayer sinusoidal channel. Site SI is the center of a hexagonal prism connecting the supercages. Site SII is the center of a plane of a hexagonal face or 6-ring of a hexagonal prism. Site SII* corresponds to displacement from site SII into a supercage. Sites SIII and SIV are respectively at the centers of 6-ring and 5-ring windows of a supercage. Site SIII* corresponds to displacement from site SIII toward the interior of a supercage, while sites SIV* and SIV′ correspond to displacement of site SIV toward the interior and toward the exterior of a supercage. Site SV is the center of a 5-ring forming an interlayer sinusoidal channel, and site SV* corresponds to displacement from site SV toward the center of a sinusoidal channel. Sites SIII′ and SV′ are displaced from sites SIII and SV away from a supercage and sinusoidal channel, respectively, and are unlikely due to space limitations.

Formation of Paramagnetic Pd Species. Several investigations have been devoted to locate Pd ions in zeolites such as X and Y and in SAPO structures such as SAPO-5, SAPO-11, and SAPO-34.[9−11,14,16,17] The cation locations depend both on the structure and on the activation treatment. The location of Pd(II) ions in $Pd(NH_3)_4^{2+}$-exchanged Na−Y zeolite was studied by X-ray diffraction.[11] At low activation temperature (<390 K) the majority of Pd(II) ions occupy site SV, which is at the center of a supercage. As the activation temperature increases, $Pd(NH_3)_4^{2+}$ ions start decomposing to form Pd(II) ions which eventually migrate toward a sodalite cage. At temperatures above 570 K most of the Pd(II) ions preferentially occupy site SI′ in a sodalite cage. In PdH−SAPO-5 and PdH−SAPO-11, Pd(II) ions can be stabilized at different sites depending on the activation temperature. ESR and ESEM studies on these SAPO materials reveal that thermal reduction at moderate temperatures (∼573 K) produces Pd(I) ions located at site SII* near a 6-ring window that constitutes a side of 12-ring (SAPO-5) or 10-ring (SAPO-11) straight channels. Thermal reduction at higher temperature (∼773 K) produces Pd(I) ions both at site SII* and at site SI at the center of a hexagonal prism. Thus, at high temperatures migration of palladium ions to a hexagonal prism from a main channel occurs. Similarly in PdH−SAPO-34, Pd(I) ions are stabilized in three different locations.

The exchange of Na−MCM-22 with $Pd(NH_3)_4Cl_2$ leads to $Pd(NH_3)_4^{2+}$ cations in a supercage and in sinusoidal channels. PdNa−MCM-22 in its hydrated state shows no ESR signal. Upon thermal treatment the $Pd(NH_3)_4^{2+}$ cation decomposes to form Pd(II) ions which are then reduced to Pd(I) by NH_3 and H_2O. Thus, the formation of Pd(I) species A after dehydration at 373 K can be explained by reaction 1.

$$2Pd(II) + H_2O \rightarrow 2Pd(I) + 2H^+ + (1/2)O_2 \qquad (1)$$

However, species A disappears upon dehydration at higher temperatures. No ESR signal is observed even after heating at 773 K. The oxygen formed in reaction 1 might produce Pd(II) cations by reaction 2.

$$2Pd(I) + H_2O + (1/2)O_2 \rightarrow 2Pd(II) + 2OH^- \qquad (2)$$

The most common oxidation states of paramagnetic palladium species are Pd(I) and Pd(III) whose electronic configuration are $4d^9$ and $4d^7$, respectively. Both Pd(I) and Pd(III) have been observed in palladium-exchanged X and Y zeolites[9,12] and have different ESR characteristics. An isotropic signal with $g = 2.22$ in PdNa−Y and $g = 2.23$ in PdCa−X is observed for Pd(III). On the other hand, an axially symmetric signal with $g_{\|} \sim 2.6$ and $g_{\perp} \sim 2.1$ is observed for Pd(I) in several palladium-exchanged zeolites and in SAPO materials.[10,16,17,24] Thus we assign species B with $g_{\|} = 2.693$ and $g_{\perp} = 2.136$ to Pd(I) produced by both thermal reduction and hydrogen reduction. The intensity of species B obtained from hydrogen reduction is higher than that observed from thermal reduction.

The mechanism for the formation of Pd(I) after oxidation and subsequent evacuation at high temperature (sample type C) is not clear. Naccache et al.[12] suggested reactions 3 and 4

$$2NH_3 + 3O_z^{2-} \rightarrow N_2 + 3H_2O + 6e^- \qquad (3)$$

$$Pd(II) + e^- \rightarrow Pd(I) \qquad (4)$$

for the formation of Pd(I) in PdNa−Y where O_z represents a zeolitic framework oxygen. This seems inconsistent with no ESR signal observed after heating PdNa−MCM-22 in vacuum at high temperature. A strong Pd(I) signal is observed only after dehydration in vacuum, followed by treatment with O_2 and subsequent evacuation at high temperature.

In Pd-exchanged X and Y zeolites (Si/Al ratios of 1.2 and 2.4) an isotropic ESR signal at $g = 2.3$ due to Pd(III) is observed. Such an isotropic ESR signal due to Pd(III) is not observed after oxidation treatment of PdNa−MCM-22. The Si/Al ratio of MCM-22 is 11.2. Pd(III) is not observed in other Pd-exchanged zeolites such as mordenite (Si/Al = 5) or K−L (Si/Al = 3) or in SAPO-5, SAPO-11, and SAPO-34.[10,13,16,17,24] The low framework negative charge of these SAPO materials may not be sufficient to stabilize the higher oxidation state of palladium. However, there are reports on the formation of Pd(III) in Pd-modified zeolites such as mordenite[13] (Si/Al = 5) or K−L[26] (Si/Al = 3).

Oxygen Adduct. In PdK−L zeolite, an ESR signal with reversed g values of $g_{\|} = 1.978$ and $g_{\perp} = 2.045$ is observed after heating the sample in flowing O_2 to 523 K. This signal was assigned to Pd(III) based on temperature-programmed reduction experiments. A similar signal is observed in PdNa−MCM-22 as Pd species C after oxygen or water adsorption on an activated sample (Figure 3). Similarly, for Pd-exchanged mordenite, Shpiro et al.[13] tentatively assigned this species with

reversed g parameters to a Pd(III)−O_2 complex based on combined ESR and XPS experiments. Pd species C with reversed g values has been observed in various palladium-modified molecular sieves formed by addition of water or O_2 to an activated sample.[9,10,16,17] This species was then assigned to Pd(II)−O_2^- radical. Although O_2^- normally has $g_{\|} > g_{\perp}$, an average rotation around the intranuclear axis of O_2 is suggested to account for the reversed g values of Pd species C. Alternatively, a Pd(II)−O_2^{3-} complex is consistent with $g_{\perp} > g_{\|}$ because O_2^{3-} is isoelectronic with Cl_2^- or F_2^-.[27] In our present study, Pd species B, which transforms to Pd species C upon O_2 adsorption, can be readily regenerated by evacuation of the sample at room temperature (Figure 2d). This indicates that oxygen is only weakly bound to palladium ion. Adsorption of water on an activated sample produces the same Pd species C after O_2 adsorption. This species has been assigned to Pd(II)−O_2^- radical formed as a result of water decomposition by Pd(I).[9] Water decomposition has been demonstrated on various zeolites with other exchangeable cations.[29,30] Analysis of the three-pulse ESEM pattern for Pd species C indicates that two deuterium nuclei interact with Pd(II)−O_2^- at a distance of 0.42 nm. This distance is larger than a direct coordination distance of 0.3 nm between Pd(I) or Cu(II) and water. Therefore, one water molecule is indirectly coordinated to Pd(II)−O_2^-.

Hydrogen Addition. The effect of hydrogen addition at room temperature to an activated sample showing Pd(I) is to increase the concentration of Pd(I). Hydrogen addition increases the concentration of Pd(I) by a factor of 10 as measured from the intensities of the ESR signal before and after H_2 adsorption. During the activation process only about 5% of the total Pd(II) is reduced to Pd(I). Thus, the enhanced intensity of Pd species B indicates further reduction of Pd(II) to Pd(I) takes place with H_2. However, heating such a sample at 573 K for 30 min generates a broad isotropic ESR signal. Such a signal has been assigned to the formation of palladium clusters in PdNa−Y zeolite.[31] It has also been postulated that temperatures higher than 500 K induce migration of Pd(0) to α-cages where they form metal agglomerates.[9] In PdCa−X zeolite, reduction by H_2 at 500 K produces both Pd(I) and Pd(0).[9] A similar mechanism in MCM-22 is also possible since the supercage in MCM-22 is comparable to the α-cage in X and Y zeolites.

CO Adsorbate. The adsorption of ^{12}CO on activated PdNa−MCM-22 results in the formation of Pd species D with a rhombic g tensor. When ^{13}CO is adsorbed, the resultant spectrum consists of three sets of three hyperfine lines (Figure 4c). Since ^{13}C has a nuclear spin of $^1/_2$ and ^{12}C of zero, the hyperfine lines of relative intensity 1:2:1 indicate two CO molecules coordinated to Pd(I) ion. A similar complex with Pd(I) has been observed in several materials such as PdNa−Y, PdK−L, and PdH−SAPO-n.[12,17,27] The site location of this complex within the zeolite seems to have no effect on the ESR characteristics of this Pd(I)$[CO]_2$ complex as there is only one species observed after CO adsorption. It is significant that Pd species B vanished upon adsorption of CO molecules. Pd species D is quite stable at room temperature as indicated by the same intensity of this species after keeping the sample at room temperature for 24 h. A new species E is observed after evacuation of the sample for 15 min. On further addition of CO this species again disappears. Similar species have been observed in PdNa−mordenite[13] and assigned to a Pd(I)−CO complex. Annealing PdNa−MCM-22 at higher temperatures transforms species D to species F. At a temperature of 773 K both species D and F vanish completely. The interaction of CO with metals such as Ru(III), Ir(III), and Pd(II) reduces these ions to Ru(I), Ir(I), and Pd(I).[13,32,33] In the present study, further reduction of Pd(I) to Pd(0) by CO is not observed.

Ethylene Adsorbate. Several new species G_1, G_2, and G_3 are observed after adsorption of ethylene on activated PdNa−MCM-22. Species G has been observed earlier in PdCa−X, PdK−L, and PdH−SAPO-n after ethylene adsorption.[9,17,24] This species has been assigned to a Pd−$(C_2H_4)_n$ complex. It has been reported that adsorption of ethylene on PdCa−X results in a single species with $g_{\|} = 2.85$ and $g_{\perp} = 2.115$. In the present study, the three signals G_1, G_2, and G_3 with well-separated parallel components and close perpendicular components probably arise due to different environments of a Pd−$(C_2H_4)_n$ complex within the MCM-22. Analysis of the ESEM data of species G after C_2D_4 adsorption suggests that one ethylene molecule is coordinated to Pd(I). This is consistent with previous results in PdH−SAPO-34.[17] Being a small pore material ethylene dimerization is quite unlikely in this material. A single species with $g_{\|} = 2.256$ and $g_{\perp} = 2.004$ is assigned to Pd(I)−C_2H_4 on the basis of ESEM data.

Besides species G, a second species H is also observed after ethylene addition. On keeping a sample at room temperature, this second species grows in intensity for a few hours. Dimerization of ethylene has been reported in medium- and large-pore molecular sieve materials. When n-butene is adsorbed on PdH−SAPO-5, an ESR signal with $g_{\|} = 2.421$ and $g_{\perp} = 2.032$ is observed.[23] On the basis of ESEM data this species is assigned to Pd(I)−C_4H_8. Similar results are reported in PdCa−X and PdCa−Y materials.[34,35] Species H has g values similar to those reported for Pd(I)−C_4H_8. A new species I is observed after heating PdNa−MCM-22 at higher temperatures. At 423 K both species H and I vanish, and a new radical species appears in the ESR spectrum. An assignment of this species H is not possible at this moment. However, because of the large supercage present in MCM-22, further dimerization of ethylene is a possibility.

Alcohol Adsorption. Adsorption of methanol on activated PdNa−MCM-22 produces a broad ESR signal (Figure 7c). Species K is similar to the signal observed after treating an activated sample with H_2 at 573 K. Thus, it is quite likely that this signal is also related to the formation of palladium clusters. Similar to the observation made in this study, adsorption of methanol on activated PdK−L results in palladium clusters.[24] However, in PdCa−X the same treatment results in a species suggested to be a Pd(I)−CH_3OD complex.[9] The same authors have reported that Pd(III) formed in PdCa−X is reduced at room temperature by methanol faster than by hydrogen. The decomposition of methanol molecules on acidic sites in the main channel with formation of atomic hydrogen may be a possible mechanism in which H atoms are responsible for the formation of Pd clusters. Alternatively, the reduction of Pd(I) may proceed via electron transfer from an adsorbate molecule to an electron acceptor site in the zeolite framework which in turn reduces the palladium cation. Note that the intensity of species B observed after methanol adsorption remains almost the same even after annealing at room temperature for 24 h (Figure 7d). This indicates that the unreacted fraction of Pd(I) is not accessible by methanol.

When ethanol is adsorbed on activated PdNa−MCM-22, species J is observed along with species B and C which is in sharp contrast to methanol adsorption. Species C is due to some water impurity in ethanol. A considerable fraction of Pd(I) does not react with ethanol. The observed difference in the adsorption behavior of methanol and ethanol is probably due to a difference in the electron donor capability. The ESEM pattern with adsorbed CH_3CH_2OD indicates one deuterium nucleus at

0.3 nm from Pd(I). This suggests that one ethanol directly coordinates to Pd(I) to form species J.

Ammonia and Pyridine Adsorption. Two new species L and M are observed after ammonia adsorption. A significant fraction of Pd(I) is not accessible to ammonia since the intensity of Pd(I) species B does not show a time -dependent change. Species L shows a weak hyperfine interaction also. ESEM data suggest that although both species L and M consist of one ammonia molecule coordinated to Pd(I), the distances observed are different. The shorter interaction distance observed for species L suggests that this species is probably situated in a sinusoidal channel. This assumption is supported by the formation of a single species when pyridine is adsorbed; this species has *g* values similar to those of species M. Since pyridine is larger than ammonia, complex formation between this pyridine and Pd(I) inside the sinusoidal channel is unlikely. Species M and N are probably formed in a supercage. ESEM data for species N are consistent with one pyridine molecule coordinating with Pd(I).

Location of Pd(I). Because of its large size, $Pd(NH_3)_4^{2+}$ cannot occupy a hexagonal prism and is most likely located inside a supercage. During thermal decomposition Pd(II) can occupy a supercage or a sinusoidal channel. During subsequent activation and reduction to Pd(I) occupation of a hexagonal prism becomes possible. When ND_3, C_2D_4, C_5D_5N, and CH_3OD, CH_3CH_2OD are adsorbed, a significant fraction of Pd(I) remains unreacted or uncomplexed. Even after keeping the sample at room temperature for long periods, the intensity of Pd(I) does not change noticeably. However, Pd(I) almost completely decays upon adsorption of O_2, D_2O, and CO. A probable explanation is that the unreacted fraction of Pd(I) is not accessible to these adsorbates which is consistent with a hexagonal prism site. The particular case of CO adsorption is an exception. Although the molecular size of CO is slightly larger than the entrance of a 6-ring window, it does reach Pd(I) species B located in a hexagonal prism. The strong electric fields present in zeolites can also produce changes in the adsorption properties. In a study of CO adsorption on PdNa−Y zeolites, Naccache et al.[12] have come to a similar conclusion from their ESR and IR results. They suggested that CO molecules penetrate a sodalite cage.

Conclusions

Formation of Pd(I) in Pd(II)−exchanged Na−MCM-22 zeolite has been monitored by ESR and ESEM spectroscopic methods. Dehydration, oxidation, and subsequent evacuation at 825 K (activation) of PdNa−MCM-22 generates Pd(I). Pd(I) ions can also be generated by hydrogen reduction of PdNa−MCM-22 after dehydration and oxidation at high temperature. Addition of hydrogen to an activated sample has two effects depending on the temperature. At room temperature there is further reduction of Pd(II) to Pd(I). At temperatures above 573 K palladium clusters are formed. Both oxygen and water have an oxidizing effect on activated PdNa−MCM-22 and generate a $Pd(II)-O_2^-$ species. Depending on the treatment conditions, two palladium complexes, $Pd(I)-(CO)_2$ and Pd(I)−CO, are formed after adsorption of CO. Two species assigned as $Pd(I)-C_2H_4$ and $Pd(I)-C_4H_8$ complexes are observed after adsorption of ethylene on activated sample, suggesting Pd-catalyzed dimerization of ethylene. Unlike observations on other Pd-exchanged zeolites, adsorbed methanol and ethanol behave differently. Methanol reduces Pd(I) to $Pd(0)_n$ at room temperature, while ethanol forms a palladium complex suggested to be $Pd(I)-CH_3CH_2OD$ based on ESEM data. Adsorption of ammonia on activated PdNa−MCM-22 leads to two Pd(I)−ND_3 complexes probably with different environments in the zeolite. On the other hand, adsorption of pyridine results only in a single species in PdNa−MCM-22 probably due to steric constraints offered by the zeolite framework. Pd(I) ions formed in the supercage during activation migrate to hexagonal prism sites which are inaccessible to relatively large molecules.

Acknowledgment. This research was supported by the National Science Foundation and the Robert A. Welch Foundation.

References and Notes

(1) Rubin, M. K.; Chu, P. U.S. Patent 4 954 325, 1990.

(2) Lawton, S. L.; Fung, A. S.; Kennedy, G. J.; Alemany, L. B.; Chang, C. D.; Hatzikos, G. H.; Lissy, D. N.; Rubin, M. K.; Timken, H.-K. C.; Steuernagel, S.; Woessner, D. E. *J. Phys. Chem.* **1996**, *100*, 3788.

(3) Leonowicz, M. E.; Lawton, J. A.; Lawton, S. L.; Rubin, M. K. *Science* **1994**, *264*, 1910.

(4) (a) Huss, Jr., A.; Kirker, G. W.; Keville, K. M.; Thomson, R. W. U.S. Patent 4 992 615, 1991**.** (b) Del Rossi, K. J.; Huss, Jr., A. U.S. Patent 5 107 047, 1992. (c) Chu, C. T.-W. U.S. Patent 4 956 514, 1990.

(5) Corma, A.; Corell, C.; Llopis, F., Martinez, A.; Perez-Pariente, J. *Appl. Catal.* **1994**, *115*, 121.

(6) Kirker, G. W.; Mizrahi, S.; Shih, S. U.S. Patent 5 000 839, 1991.

(7) (a)Kolodziejski, W.; Zicovich-Wilson, C.; Corell, C.; Perez-Pariente, J.; Corma, A. *J. Phys. Chem.* **1995**, *99*, 7002. (b) Absil, R. P. L.; Bowes, E.; Green, G. J.; Marler, D. O.; Shihabi, D. S.; Socha, R. F. U.S. Patent 5 085 762, 1992.

(8) Prakash, A. M.; Kevan, L. *J. Phys. Chem.* **1996,** *100*, 19587.

(9) Michalik, J.; Narayana, M.; Kevan, L. *J. Phys. Chem.* **1985**, *89*, 4553.

(10) Lee, C. W.; Yu, J. S.; Kevan, L. *J. Phys. Chem.* **1992**, *96*, 7747.

(11) Bergeret, G.; Tri, T. M.; Gallezot, P. *J. Phys. Chem.* **1983**, *87*, 1160.

(12) Naccache, C.; Primet, M.; Mathieu, M. V. *Adv. Chem. Ser.* **1973**, *121*, 2661.

(13) Shipiro, E. S.; Baeva, G. N.; Sass, A. S.; Shvets, V. A.; Fasman, A. B.; Kazanskii, V. B.; Minachev, Kh. M. *Kinet. Catal. (Engl. Transl.)* **1988**, *28*, 1236.

(14) Narayana, M.; Michalik, J.; Contarini, S.; Kevan, L. *J. Phys. Chem.* **1985**, *89*, 3895.

(15) Kevan, L. *Acc. Chem. Res.* **1987**, *20*, 1

(16) Yu. J. S.; Kurshev, V.; Kevan, L. *J. Phys. Chem.* **1994**, *98*, 10225.

(17) Back, G. H.; Yu, J. S.; Kurshev, V.; Kevan, L. *J. Chem Soc., Faraday Trans.* **1994**, *90*, 2283.

(18) Bolton, A. P. In *Zeolite Chemistry and Catalysis*; Rabo, J. A., Ed.; American Chemical Society: Washington, DC, 1976; Chapter 13.

(19) Thomson, R. T.; Wolf, E. E. *Appl. Catal.* **1988**, *41*, 65.

(20) Lapidus, A. L.; Mal'tsev, V. V. *Acta Phys. Chem.* **1978**, *24*,195.

(21) Ghosh, A. K.; Kevan, L. *J. Phys. Chem.* **1988**, *92*, 4439.

(22) Hunger, M.; Ernst, S.; Weitkamp, J. *Zeolites* **1995**, *15*, 188.

(23) Hartmann, M.; Kevan, L. *J. Phys. Chem.* **1996**, *100*, 4606.

(24) Yu, J. S.; Kevan, L. *Langmuir* **1995**, *11*, 1617.

(25) Smith, J. V. In *Zeolite Chemistry and Catalysis*; Rabo, J. A., Ed.; American Chemical Society: Washington, DC, 1976, Chapter 1.

(26) Ganghi, S. N.; Lei, G. D.; Sachtler, W. M. H. *Catal. Lett.* **1993**, *17*, 117.

(27) Yu, J. S.; Comets, J. M.; Kevan, L. *J. Chem. Soc., Faraday Trans.* **1993**, *89*, 4397.

(28) Kasai, P. H.; Bishop Jr., R. J. *J. Phys. Chem.* **1977**, *81*, 1527.

(29) Azuma, N.; Kevan, L. *J. Phys. Chem.* **1995**, *99*, 5083.

(30) Lee, C. W.; Saint-Pierre, T.; Azuma, N.; Kevan, L. *J. Phys. Chem.* **1993**, *97*, 11811.

(31) Bergeret, G.; Gallezot, P.; Imelik, B. *J. Phys. Chem.* **1981**, *85*, 411.

(32) Naccache, C.; Lefebvre, F.; Gelin, P.; Taarit, Y. B. In *Organic Reactions in Organic and Inorganic Constrained Systems*; Setton, R., Ed.; D. Reidel: Dordrecht, 1986; p 81.

(33) Primet, M.; Vedrine, J. C.; Naccache, C. *J. Mol. Catal.* **1978**, *4*, 411.

(34) Ghosh, A. K.; Kevan, L. *J. Phys. Chem.* **1989**, *93*, 3747.

(35) Ghosh, A. K.; Kevan, L. *J. Am. Chem. Soc.* **1988,** *110*, 8044.